Digital Discovery

ROYAL SOCIETY OF CHEMISTRY

PAPER

View Article Online
View Journal

Cite this: DOI: 10.1039/d5dd00554j

Python-controlled, solvent-resistant fraction collector for automated flow synthesis

Hongchen Wang,[ab] Owen A. Meville,[b] Harrison A. Mills,[b] Monique Ngan,[b] Jay R. Werber[bc] and Nipun Kumar Gupta *[b]

Flow chemistry has emerged as a powerful approach for high-throughput and automated synthesis workflows. However, downstream fraction collection remains a practical challenge: commercial systems are often expensive and difficult to integrate, while most low-cost or DIY alternatives lack compatibility with common organic solvents and real-time control. Here, we present a solvent-resistant, Python-controlled fraction collector built from low-cost, modular components (~$1000). The system integrates programmable vial positioning and real-time volumetric monitoring to enable accurate, flow-independent fraction collection. Performance was validated across a range of flow rates (0.1–6 mL min^{-1}) and viscosities (0.45–500 cP), with consistent droplet mass and high reproducibility. It also achieves high separation fidelity, with sharp fluid transitions and negligible carryover between fractions under both aqueous and organic conditions. This open-source platform offers a robust, integrable solution for automated flow synthesis and supports broader adoption of continuous, data-rich experimentation in organic chemistry.

Received 11th December 2025
Accepted 19th April 2026

DOI: 10.1039/d5dd00554j

rsc.li/digitaldiscovery

Introduction

Automation and machine learning are emerging as valuable tools in modern chemistry, but much work remains to make these tools accessible and affordable. Automated chemical synthesis and characterisation platforms often rely on flow-based systems to accelerate research.[1–3] Unlike traditional batch chemistry, flow-based systems are relatively straightforward to automate, enabling precise, automated tuning of reaction parameters and making them especially advantageous for reactions requiring tight control or hazardous conditions.[4–8] This has made flow chemistry attractive for organic synthesis, including polymers, macromolecules, and pharmaceuticals, as well as automated reaction screening.[9–13] Whilst such physically interconnected systems are amenable to automation, sample isolation for characterisation and further downstream processing is essential for most processes, especially at the end of the workflow. Accurate, reproducible sample collection is essential not only for monitoring reaction performance but also for ensuring that downstream steps, such as NMR or chromatographic characterisation, receive consistent sample inputs.[14,15]

Fraction collectors can assist in this integration by automatically separating samples eluting from a flow-based system. This eliminates the need for researchers to manually gather reaction products at the end of each iteration, reducing human error and enabling uninterrupted, high-throughput experimentation.[16] Most chemistry-focused commercial fraction collectors are expensive and may be challenging to integrate into automated experimental systems.[16] On the other hand, most of the more budget-friendly fraction collectors presented in the literature are designed for aqueous chemistry or chromatography setups,[16–20] and are incompatible with harsh organic solvents (*e.g.*, tetrahydrofuran (THF), toluene, chloroform), which are heavily utilised in organic synthesis. They may also rely on pre-programmed flow rate and timing rather than real-time feedback, which could potentially yield inaccurate collection when a reactant or product is in the gaseous phase or has high viscosity.[21] Thus, there is a strong need for a fraction collector that is automatable, customisable according to project needs, and resistant to the most common organic solvents.

Computer numerical control (CNC) machines, which use a precise XYZ gantry to move an integrated toolhead, have been repurposed to hold research tools for low-cost lab automation.[22–25] For example, Monterrubio *et al.*[22] designed a CNC-based liquid handler to enhance the reproducibility and throughput of inorganic materials synthesis. Similarly, Quinn *et al.*[23] integrated liquid handling with electrochemical and optical characterisation to perform closed-loop exploration of functional polymer films. These systems are generally compatible with Python-based or microcontroller-level control systems and offer a compact, cost-effective, and flexible alternative to commercial robotics.

[a]*Department of Materials Science and Engineering, University of Toronto, Canada*
[b]*Acceleration Consortium, University of Toronto, Canada. E-mail: nipun.gupta@utoronto.ca*
[c]*Department of Chemical Engineering, University of Toronto, Canada*

Table 1 BoM for constructing the fraction collector

Item	Manufacturer	Part no.	Qty	Specifications	Unit cost (USD)	Notes
CNC router	Genmitsu	3018-PROVer V2	1	425 × 352 × 300 mm	228.65	Main platform
Selector valve	Runze fluid	QHF-SV04M-B-X-U-T10-K1.2 C	1	10 Port or 6 Port	414	Switching between waste and collection
Drop counter	Vernier®	GDX-DC	1	Go direct®	206	For drop counting
Fixture	N/A	N/A	1	Custom 3D-Printed	2	For integrating modules
Tubing	IDEX	1502	≥5 ft	1/16″ OD × 0.030″ ID, PFA	28.45	Tubing
Flangeless nut	IDEX	P-245	≥5	1/4-28, PFA	3.36	Tubing connector
Ferrule	IDEX	P-200N	≥5	1/4-28 for 1/16″ OD, ETFE	1.79	Tubing connector

Herein, we developed a solvent-resistant, Python-controlled fraction collector compatible with a wide range of flow chemistry applications, including but not limited to organic synthesis. Built from modular, low-cost components (~$1000 total), the system integrates with upstream flow reactors. All wetted components are made of fluoropolymer materials, and are compatible with common organic solvents, including THF, acetone, toluene, dichloromethane, and ethyl acetate. The system is built on a benchtop CNC platform that provides programmable three-axis motion for precise vial positioning and flexible layout configurations. A chemically resistant selector valve programmatically toggles fluid output between waste and collection modes, eliminating manual intervention and minimising cross-contamination. The fraction collector features a drop counter for independent control of each fraction's volume and a compact form factor that can be easily integrated into a standard chemistry fume cupboard. It also provides real-time feedback on dispensed volume, enabling reliable droplet detection and reproducible collection regardless of pump calibration or flow irregularities. Across replicate experiments, the system achieved a coefficient of variation (CV) of 1.3% in the fitted drop mass, indicating high precision and repeatability. The collector ensures clean separations between samples and can be customised for diverse laboratory setups. The system supports high-throughput experimentation by simplifying fraction collection and facilitating the generation of large sample libraries to accelerate reaction discovery and modelling.

Experimental

Materials

The chemicals we used for the experiments conducted in this study are acetone (67-64-1, Sigma-Aldrich), isopropanol (IPA, 67-63-0, Sigma-Aldrich), chloroform (67-66-3, Sigma-Aldrich), 5-norbornene-2,3-dicarboxylic anhydride (826-62-0, TCI), ethyl acetate (141-78-6, Fisher Chemical), piperidine (110-89-4, Sigma-Aldrich), toluene (108-88-3, Sigma-Aldrich), tetrahydrofuran (THF, 109-99-9, Sigma-Aldrich).

The bill of materials (BoM) for constructing the fraction collector is shown in Table 1 below. The assembly guide is provided in the GitHub repository.

Droplet consistency across flowrate and viscosity. It is essential to verify that the system can maintain accurate droplet mass and reliable detection across a practical range of flow conditions, as volume-based fraction collection relies heavily on stable droplet formation. To assess the sensitivity, accuracy, and droplet-mass consistency of the fraction collector, we performed experiments to probe the system's response to controlled variations in flow rate and fluid viscosity. We utilised a Vapourtec R2C+ pumping module to pump all solvents, standards, and reagents.

For the flow rate test, IPA (viscosity ≈ 2.2 cP at 25 °C) was used as the reference fluid. The R2C+ pump dispensed IPA at controlled rates ranging from 0.1 to 6 mL min^{-1}, while the drop counter and a precision balance simultaneously logged drop counts and cumulative weight in real time. Each condition was repeated three times, and the resulting droplet weights were recorded to assess accuracy, consistency, and timing precision across different flow conditions.

For the viscosity tests, Siltech viscosity standards ranging from 1 to 500 cP and ethyl acetate (0.45 cP) were dispensed at 1 mL min^{-1}. Each viscosity test was repeated three times to assess whether the drop counter could reliably register droplets under varying viscosities.

Fraction accuracy *via* food dye. We designed a colour-switching experiment using four visually distinct food dyes (red, blue, yellow, and green) to evaluate the fraction collector's separation accuracy. These dyes are ideal for validating fraction purity because any cross-contamination produces easily detectable spectral signatures.

The dyes were sequentially dispensed with the R2C+ pump at a constant flow rate of 1 mL min^{-1}. The samples were collected into a well plate by the fraction collector following predefined timing intervals. Each sequence of four colours was repeated three times to assess reproducibility and any cross-contamination between consecutive fractions. The collected fractions were then analysed using a Cytation 5 plate reader to record their absorbance spectra across the visible wavelength range. Reference spectra for each pure dye solution were measured under identical conditions to serve as baselines.

Chemical reactions and analyses. To validate the operational accuracy of the fraction collector in an organic synthesis setting, we selected the aminolysis of nadic anhydride (5-norbornene-2,3-dicarboxylic anhydride) with piperidine as a model transformation. This reaction proceeds *via* nucleophilic ring-opening of the anhydride, yielding an amide–carboxylic acid product. The reaction was conducted in a Vapourtec R2C+ flow

reactor with two 5 mL reactor coils (total reactor volume 10 mL) and two pumps at 60 °C using anhydrous THF as the solvent. 0.9 M nadic anhydride and 1.0 M piperidine solutions in THF were connected to pumps 1 and 2, respectively. A flow rate of 0.25 mL min^{-1} was applied to both reactants, and the total flow rate was set to 0.5 mL min^{-1} using a backpressure regulator (set at 8 bar) to maintain system stability, resulting in a total residence time of 20 min. Once steady-state conditions were established, three consecutive 1 mL fractions were collected using the fraction collector.

Each collected fraction was evaporated using a rotary evaporator and redissolved in 1 mL of $CDCl_3$. A 200 μL aliquot was then mixed with 50 μL of a 20 mM ferrocene internal standard solution in DMSO-d_6. To reduce proton exchange effects between the solvent and the product carboxylic acid, 100 μL of DMSO-d_6 was added to the Nuclear magnetic resonance spectroscopy (NMR) sample to suppress broadening of the COOH peak. A 350 μL volume of the final solution was transferred to a 3 mm NMR tube for analysis.

Quantitative ^{1}H NMR spectra were recorded on a Bruker Ascend 400 MHz NMR spectrometer equipped with a liquid N_2-cooled cryoprobe. A pulse angle of 30° was used, with a relaxation delay (d1) of 35 seconds, calculated to be at least 7 times the longitudinal relaxation time ($T_1 = 4.9$ s) of ferrocene to ensure full relaxation and accurate quantification. Spectra were acquired at 25 °C and referenced to residual proton signals of d-DMSO (δ 2.50 ppm). Product concentration was determined relative to the ferrocene integral to allow direct calculation of product yield.

Results and discussion

Design of a drop counter-based fraction collector

We developed a solvent-resistant fraction collector built from low-cost, modular components (Fig. 1A) to enable accurate, automated volume-based sampling in flow-based systems. The system is based on a benchtop CNC machine that provides precise, programmable XYZ motion for toolhead and vial positioning. A solvent-resistant programmable selector valve directs fluid flow to either waste or sample vials, enabling automated switching between collection states without manual intervention. A drop counter allows real-time, precise volume tracking independent of flow rate or pump timing, particularly important when handling variable flow conditions. It also serves as a compact and inexpensive alternative to continuous high-precision weighing. A 3D-printed fixture integrates the selector valve and drop counter to the CNC machine and aligns the dispensing tubing directly over each vial. This design enables precise and flexible access to a large array of collection vials while minimising cross-contamination between samples.

Fig. 1B shows the process schematics and workflow. Once flow is initiated from the upstream reactor, fluid enters the selector valve, which is used to programmatically switch the output stream between waste and sample collection. Initially, the system is set to direct flow to waste until the reaction reaches steady state. Upon reaching steady-state, the toolhead moves to a local waste container placed on the CNC platform and switches the valve to direct fluid through the drop counter, rinsing the collection tubing with a defined number of drops. After rinsing, the toolhead transitions to the target sample vial location (in this case, on a 48-well plate); during this transition, the valve temporarily switches back to waste to prevent unwanted dripping. Once in position, the valve is switched to collection mode, and droplet counting begins. Droplet counts are continuously logged during this stage to allow precise volume measurement and real-time feedback for flow control. Once the target number of drops is reached, the system automatically switches the selector valve back to waste until the next collection event.

Both the timing of fraction transitions and the required rinsing duration can be programmatically defined using the tubing length, inner diameter, and flow rate, allowing the system to be adapted to different fluidic setups. All fluid-handling operations and toolhead motions are controlled

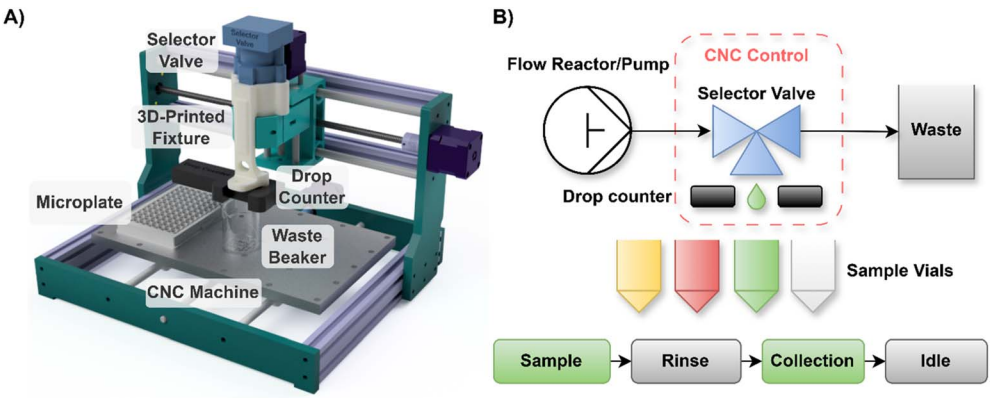

Fig. 1 Schematic and hardware overview of the solvent-resistant, Python-controlled fraction collector. (A) CAD rendering of the system, built on a 3-axis CNC platform for automated vial positioning, with a drop counter for real-time volume monitoring and a 3D-printed fixture securing the selector valve. (B) Functional flow diagram showing integration with upstream flow reactors or pumps. A selector valve alternates between sample collection and waste modes. Droplet formation is monitored by the drop counter, enabling accurate, volume-based fraction collection into user-defined sample vials. The bottom sequence illustrates the programmable collection cycle used to prevent cross-contamination.

through a Python script that also logs droplet counts and timestamps for each sample. All the wetted components are made of fluoropolymers and are chemically resistant, allowing compatibility with aggressive organic solvents such as tetrahydrofuran (THF), dichloromethane (DCM), acetone, and chloroform. This enables broad applicability across both aqueous and organic synthesis workflows without hardware degradation or failure.

Collection accuracy across varying flow rates and viscosities

It is critical to determine whether the fraction collector can reliably perform volume-based collection across a range of flow rates, as real-world applications utilise a broad range of flow rates. Fig. 2 presents the cumulative weight plotted against drop count for IPA dispensed from 0.1 to 6.0 mL min^{-1}, with three replicates measured at each flow rate. The curves exhibit a consistent linear relationship and show substantial overlap both across replicates and between different flow rates.

From the slopes of these linear fits, we determined an average droplet weight of 8.0 ± 0.5 mg. The mean droplet mass varies modestly with flow rate, rising from 0.1 mL min^{-1} to approximately 3 mL min^{-1} and then decreasing slightly at higher rates. This trend forms a broad central plateau, indicating relatively stable droplet formation across most of the tested range. The low standard deviation observed within each flow-rate group confirms that the drop counter provides consistent, repeatable measurements. The strong linear relationship between measured cumulative weight and drop counts demonstrates the high sensitivity and precision of the drop counter across the range of flow rates. However, at flow rates beyond a practical limit (*i.e.*, above ~8 mL min^{-1}), the liquid is more likely to exit the tubing as a continuous stream rather than as discrete droplets, which compromises drop detection. In such cases, it may be necessary to have larger tubing inner diameters to increase the cross-sectional area and reestablish stable droplet formation.

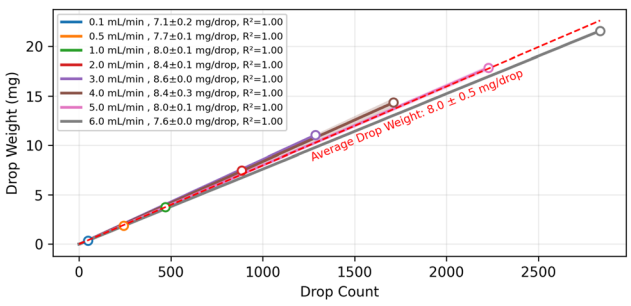

Fig. 2 Collection accuracy tests of the fraction collector at different flow rates using IPA. The plot shows the relationship between the number of drops recorded by the drop counter and the corresponding collected weight at flow rates ranging from 0.1 to 6.0 mL min^{-1}. Each curve represents a different flow rate, with the associated droplet weight and linear fit (R^2) summarised in the legend. Shaded regions represent the standard deviation across replicates for each flow rate. The average drop weight across the range of flow rates is shown as the red dashed line and the annotation.

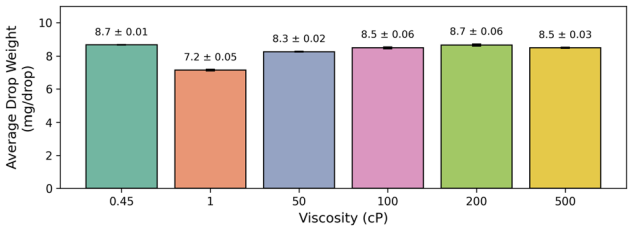

Fig. 3 Average droplet weight measured by the drop-counter-based fraction collector at different fluid viscosities. Each bar represents the mean droplet weight obtained from three repeated tests using Siltech viscosity standards ranging from 1 to 500 cP and ethyl acetate (0.45 cP). Error bars indicate the standard deviation of droplet weight for each viscosity condition. The error bars represent the standard deviation calculated from three independent experiments.

Fig. 3 presents the droplet weights measured across fluids spanning more than two orders of magnitude in viscosity. Despite large differences in viscosity (*i.e.*, 0.45 cP to 500 cP), the measured droplet weights remain within a relatively narrow range (~7–9 mg per drop), with moderate variation between fluids. The small standard deviations within each viscosity group (typically <0.1 mg per drop) indicate that the drop counter consistently detects discrete droplets even when fluid rheology differs substantially.

The observed variance between fluids may be influenced by factors including pump compliance, fluid density, viscosity, and interfacial properties.[26,27] In the present study, the relatively larger deviation observed for the 1 cP standard is consistent with its lower density compared with the other Siltech viscosity standards used, which otherwise have more similar densities across the higher-viscosity range. It was also qualitatively observed that higher viscosity fluids sometimes exhibited pulsation issues and reduced flow rates, likely due to increased backpressure and mechanical limitations of the pumping system. In the quasi-static regime, droplet detachment is governed primarily by the balance between gravity and surface tension, and therefore droplet size is expected to depend on fluid properties such as surface tension and wetting behaviour rather than viscosity alone.[28–30] As a result, different solvents or additives may yield different droplet volumes under otherwise identical conditions. The system does not assume a fixed droplet volume across fluids, as the effective drop mass can be empirically determined and, if needed, calibrated using reference measurements (*e.g.*, gravimetric analysis) for fluids with more extreme interfacial properties. Overall, the results suggest that the fraction collector is compatible with a broad range of liquids, including fluids more viscous than typical organic reaction mixtures, and can support practical volume-based fraction collection across diverse flow-chemistry conditions while allowing fluid-specific calibration when needed.

Quality of separation

Fig. 4 shows the absorbance spectra of the coloured solutions collected by the fraction collector. The characteristic peaks of each colour are labelled by the dashed lines. The strong

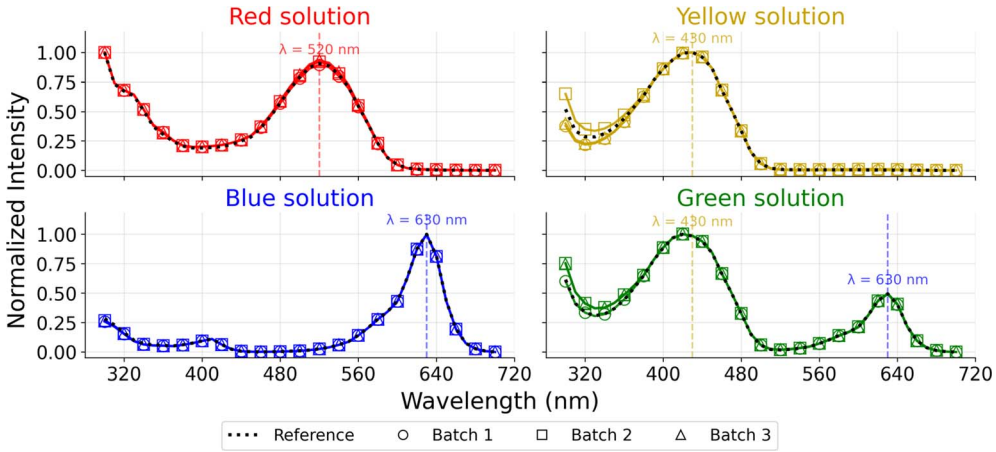

Fig. 4 Absorbance spectra of food dye solutions collected by the fraction collector across three repeated batches. Each subplot shows the normalised absorbance intensity of the red, yellow, blue, and green dye solutions, measured using a plate reader. Dotted lines indicate reference spectra for each pure dye, while markers represent three independent collection batches. Characteristic absorption peaks of the colours are indicated as vertical dashed lines at $\lambda = 520$ nm (red), $\lambda = 430$ nm (yellow), and $\lambda = 630$ nm (blue).

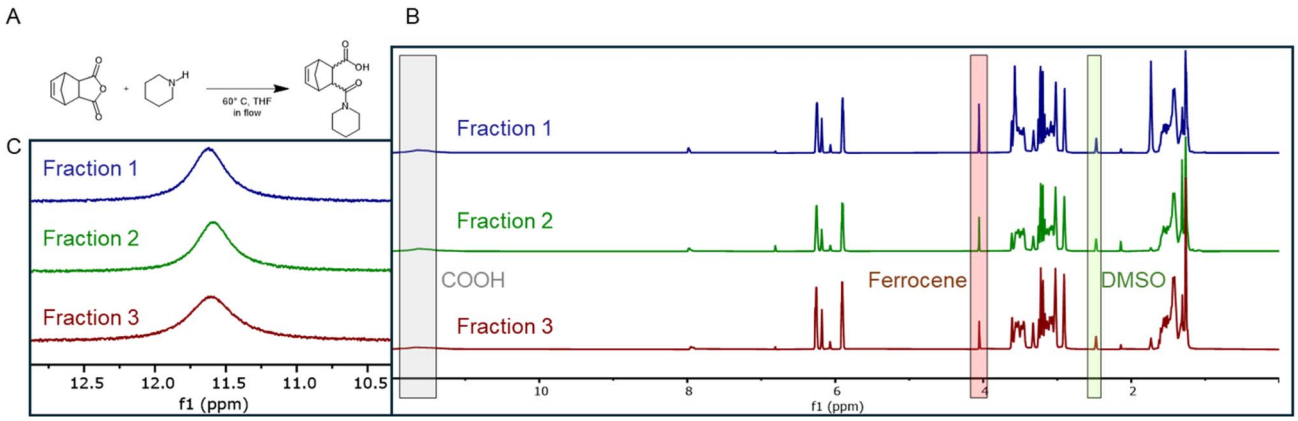

Fig. 5 (A) Reaction scheme showing ring-opening of nadic anhydride with piperidine to form the amide-carboxylic acid product. (B) Overlay of ^{1}H NMR spectra (normalised to ferrocene internal standard) for three consecutive fractions collected at steady state. Key peaks highlighted: ferrocene (4.0 ppm, red box), DMSO-d_6 solvent (2.5 ppm, green box), and carboxylic acid proton (11.6 ppm, grey box). (C) Expanded view of the COOH region (10.5–12.5 ppm) showing excellent consistency across all three fractions (integrations: 5.51, 5.57, and 5.44 with reference to the ferrocene peak, set to 1.00).

alignment between the collected spectra and the reference measurements indicates that the expected absorption peaks for the red (~520 nm), yellow/green (~430 nm), and blue (~630 nm) dyes are clearly preserved across all three batches. The spectra show close overlap and no additional or intermediate peaks, indicating that each fraction contained only the intended dye.

These results demonstrate that the system achieves effective separation of sequential aqueous samples, with negligible cross-contamination between consecutive fractions. The consistency across the three independently collected batches reflects the robustness and reproducibility of the program-controlled collection scheme, showing that the timing intervals and valve-switching logic are sufficiently precise for repeated use. The absence of intermediate colour peaks also indicates that the rinsing steps effectively remove residual previous samples in the tubing, preventing measurable carryover between fractions.

Table 2 Summary of product yield and production rate for the collected fractions

Fraction	Product (μmol)	Yield (%)	Flow rate (mL min^{-1})	Collection time (min)	Production rate (μmol min^{-1})
1	275.50	55.10	0.5	2	137.75
2	278.50	55.70	0.5	2	139.25
3	272.00	54.40	0.5	2	136.00

To validate the fraction collector's performance with organic synthesis, we selected the aminolysis of nadic anhydride (5-norbornene-2,3-dicarboxylic anhydride) with piperidine as a model reaction. This reaction produces an amide-carboxylic acid product *via* nucleophilic ring-opening of the anhydride. The reaction was conducted in a heated flow reactor (60 °C, THF solvent, total flow rate 0.5 mL min^{-1}) and, after achieving steady-state operation, three consecutive 1 mL fractions were collected. Each fraction was dried *in vacuo*, redissolved in a deuterated solvent with ferrocene as an internal standard, and analysed by quantitative ^{1}H NMR spectroscopy, enabling direct calculation of product concentration, yield, and production rate. The reaction scheme and representative NMR spectra are shown in Fig. 5, with quantitative results summarised in Table 2.

After normalisation to the internal ferrocene standard, the COOH peaks exhibited nearly identical integrations (*i.e.*, 5.51, 5.57, and 5.44) across the fractions (average yield = 55.1 ± 0.9%). This result underscores the collector's precision in volumetric sample separation and its compatibility with downstream NMR analysis. The uniform product distribution confirms that the fraction collector maintains consistent sampling volumes and negligible cross-contamination between fractions, validating its suitability for quantitative monitoring of continuous flow synthesis. Together, the high level of agreement in both spectral and quantitative data confirms the collector's accuracy, reproducibility, and operational suitability for automated flow synthesis, highlighting its strong potential for integration into high-throughput and autonomous chemical platforms.

Conclusions

We have developed and validated a low-cost, Python-controlled fraction collector capable of accurate, real-time volume-based sampling in continuous flow chemistry setups. By integrating programmable hardware, real-time feedback, and open-source control, the collector provides a flexible platform adaptable to diverse laboratory workflows and automation pipelines. The system's solvent-resistance enables compatibility with common organic solvents (*e.g.*, THF, toluene, chloroform) used in synthesis, overcoming a key limitation of most budget fraction collectors, which are restricted to aqueous or mild conditions. Through testing across different flow rates and viscosities, the system demonstrated largely consistent droplet mass and detection sensitivity, ensuring robust performance under varied reaction conditions. High-fidelity separation and reproducibility were confirmed by visible-dye experiments and quantitative NMR analysis of a representative organic synthesis, verifying separation quality and reproducibility under both aqueous and organic conditions. This work lowers the hardware barrier to entry for chemists interested in high-throughput experimentation and autonomous synthesis, making advanced fraction collection more accessible to a broader research community. Future work may include the design of a vial-capping feature to automate HPLC or SEC sample preparation, integration with in-line analytics, and machine learning-guided optimisation loops.

Conflicts of interest

The authors declare that they have no known competing financial interests or personal relationships that could have appeared to influence the work reported in this paper.

Data availability

Data, code, and the hardware assembly guide associated with this work are publicly available on GitHub at https://github.com/AccelerationConsortium/Frac-Collector.git and archived on Zenodo at https://doi.org/10.5281/zenodo.19599205.

Acknowledgements

The authors acknowledge Stanley Lo for assistance with NMR analysis, and Niher Sarker and Allison Suichies for support with 3D printing. The authors acknowledge Prof. Jason Hattrick-Simpers for his advice throughout the project. This research was undertaken, in part, thanks to funding provided to the University of Toronto's Acceleration Consortium by the Canada First Research Excellence Fund (CFREF-2022-00042).

References

1 D. T. McQuade and P. H. Seeberger, Applying Flow Chemistry: Methods, Materials, and Multistep Synthesis, *J. Org. Chem.*, 2013, **78**(13), 6384–6389, DOI: 10.1021/jo400583m.
2 C. A. Hone and C. O. Kappe, Towards the Standardization of Flow Chemistry Protocols for Organic Reactions, *Chem.:Methods*, 2021, **1**(11), 454–467, DOI: 10.1002/cmtd.202100059.
3 R. W. Epps, A. A. Volk, K. Abdel-Latif and M. Abolhasani, An automated flow chemistry platform to decouple mixing and reaction times, *React. Chem. Eng.*, 2020, **5**(7), 1212–1217, DOI: 10.1039/D0RE00129E.
4 G. C. Lyall-Brookes, A. G. Padgham and A. Slater, Flow chemistry as a tool for high throughput experimentation, *Digital Discovery*, 2025, **4**(9), 2364–2400, DOI: 10.1039/D5DD00129C.
5 R. Porta, M. Benaglia and A. Puglisi, Flow Chemistry: Recent Developments in the Synthesis of Pharmaceutical Products, *Org. Process Res. Dev.*, 2016, **20**(1), 2–25, DOI: 10.1021/acs.oprd.5b00325.
6 L. Capaldo, Z. Wen and T. Noël, A field guide to flow chemistry for synthetic organic chemists, *Chem. Sci.*, 2023, **14**(16), 4230–4247, DOI: 10.1039/D3SC00992K.
7 M. Guidi, H. Seeberger P and K. Gilmore, How to approach flow chemistry, *Chem. Soc. Rev.*, 2020, **49**(24), 8910–8932, DOI: 10.1039/C9CS00832B.
8 K. Liu, J. Meng and X. Jiang, Gram-Scale Synthesis of Sulfoxides via Oxygen Enabled by Fe(NO3)3·9H2O, *Org.*

Process Res. Dev., 2023, **27**(7), 1198–1202, DOI: 10.1021/acs.oprd.2c00390.

9 D. J. Walsh, D. A. Schinski, R. A. Schneider and D. Guironnet, General route to design polymer molecular weight distributions through flow chemistry, *Nat. Commun.*, 2020, **11**(1), 3094, DOI: 10.1038/s41467-020-16874-6.

10 N. Zaquen, M. Rubens, N. Corrigan, J. Xu, P. B. Zetterlund, C. Boyer, *et al.*, Polymer Synthesis in Continuous Flow Reactors, *Prog. Polym. Sci.*, 2020, **107**, 101256, DOI: 10.1016/j.progpolymsci.2020.101256.

11 N. Mukhin, P. Jha and M. Abolhasani, The role of flow chemistry in self-driving labs, *Matter*, 2025, **8**(7), 102205, DOI: 10.1016/j.matt.2025.102205.

12 R. S. A. E. Ali, J. Meng and X. Jiang, Multimode Photo-CSTR (Continuous Stirred Tank Reactor) Setup for Heterogeneous Photocatalytic Processes, *Org. Process Res. Dev.*, 2024, **28**(5), 1683–1689, DOI: 10.1021/acs.oprd.3c00328.

13 L. Ji, J. Meng, C. Li, M. Wang and X. Jiang, From Polyester Plastics to Diverse Monomers via Low-Energy Upcycling, *Advanced Science*, 2024, **11**(25), 2403002, DOI: 10.1002/advs.202403002.

14 H. L. D. Hayes and C. J. Mallia, Continuous Flow Chemistry with Solids: A Review, *Org. Process Res. Dev.*, 2024, **28**(5), 1327–1354, DOI: 10.1021/acs.oprd.3c00407.

15 M. A. Morin, D. Mallik, W. Zhang, W. Pietro, J. M. Manthorpe and M. G. Organ, Obtaining Kinetics From Continuous Processes: Sampling Multiple Time Points Concurrently With a Single Valve Rotation, *Chem.:Methods*, 2021, **1**(2), 131–134, DOI: 10.1002/cmtd.202100003.

16 A. S. Booeshaghi, Y. Kil, K. H. Min, J. Gehring and L. Pachter, Low-cost, scalable, and automated fluid sampling for fluidics applications, *HardwareX*, 2021, **10**, e00201, DOI: 10.1016/j.ohx.2021.e00201.

17 F. Bravo-Collazo, G. Guerrero-Mora, G. González-Badillo and E. Maldonado-Cervantes, Design and construction of a fraction collector for liquid chromatography, *Ing. Investig. Tecnol.*, 2024, **25**(1), DOI: 10.22201/fi.25940732e.2024.25.1.007.

18 W. J. Crandall, M. Caputo, L. Marquez, Z. R. Jarrell and C. L. Quave, Customizable large-scale HPLC fraction collection using low-cost 3D printing, *HardwareX*, 2025, **21**, e00612, DOI: 10.1016/j.ohx.2024.e00612.

19 D. Díaz, A. de la Iglesia, F. Barreto and R. Borges, DIY Universal Fraction Collector, *Anal. Chem.*, 2021, **93**(27), 9314–9318, DOI: 10.1021/acs.analchem.1c01519.

20 Y. Chen, C. Desmons, M. Cattoen and J. C. M. Monbaliu, Open-source fraction collector for flash column chromatography and continuous flow reactions, *React. Chem. Eng.*, 2025, **10**(6), 1408–1416, DOI: 10.1039/D5RE00070J.

21 A. S. Kaplitz, T. A. Berger, B. K. Berger and K. A. Schug, A review of fraction collection technology for supercritical fluid chromatography, *TrAC, Trends Anal. Chem.*, 2022, **151**, 116588, DOI: 10.1016/j.trac.2022.116588.

22 I. Monterrubio, J. Orive, M. Ismail, E. Castillo, J. García, I. Redondo, *et al.*, Affordable Automated Modules for Lab-Scale High-Throughput Synthesis of Inorganic Materials, *Chemistry*, 2025, **31**(52), e02072, DOI: 10.1002/chem.202502072.

23 H. Quinn, G. A. Robben, Z. Zheng, A. L. Gardner, J. G. Werner and K. A. Brown, PANDA: a self-driving lab for studying electrodeposited polymer films, *Mater. Horiz.*, 2024, **11**(21), 5331–5340, DOI: 10.1039/D4MH00797B.

24 D. List, A. Gardner, I. Claure, J. Y. Wong and K. A. Brown, ASMI: An automated, low-cost indenter for soft matter, *HardwareX*, 2024, **20**, e00601, DOI: 10.1016/j.ohx.2024.e00601.

25 J. Vasquez, H. Twigg-Smith, J. Tran O'Leary and N. Peek, Jubilee: An Extensible Machine for Multi-tool Fabrication, in. *Proceedings of the 2020 CHI Conference on Human Factors in Computing Systems*, Association for Computing Machinery, New York, NY, USA, 2020, p. 1–13, DOI: 10.1145/3313831.3376425.

26 P. C. Rijo, J. M. O. Cremonezzi, R. J. E. Andrade and F. J. Galindo-Rosales, Correlation between the rheology of electronic inks and the droplet size generated from a capillary nozzle in dripping regime, *Phys. Fluids*, 2023, **35**(9), 093116, DOI: 10.1063/5.0166228.

27 B. Chang, G. Nave and S. Jung, Drop formation from a wettable nozzle, *Commun. Nonlinear Sci. Numer. Simulat.*, 2012, (5), 2045–2051, DOI: 10.1016/j.cnsns.2011.08.023.

28 J. Eggers, Nonlinear dynamics and breakup of free-surface flows, *Rev. Mod. Phys.*, 1997, **69**(3), 865–930, DOI: 10.1103/RevModPhys.69.865.

29 P. H. Tsai and A. B. Wang, Classification and Prediction of Dripping Drop Size for a Wide Range of Nozzles by Wetting Diameter, *Langmuir*, 2019, **35**(13), 4763–4775, DOI: 10.1021/acs.langmuir.8b04228.

30 B. He, S. Yang, Z. Qin, B. Wen and C. Zhang, The roles of wettability and surface tension in droplet formation during inkjet printing, *Sci. Rep.*, 2017, **7**(1), 11841, DOI: 10.1038/s41598-017-12189-7.